Construction and Building Materials 220 (2019) 161–176

Contents lists available at ScienceDirect

Construction and Building Materials

journal homepage: www.elsevier.com/locate/conbuildmat

Eriobotrya japonica Lindl leaves extract application for effective corrosion mitigation of mild steel in HCl solution: Experimental and computational studies

Saman Nikpour [a], Mohammad Ramezanzadeh [a], Ghasem Bahlakeh [b,*], Bahram Ramezanzadeh [a,*], Mohammad Mahdavian [a]

[a] Department of Surface Coatings and Corrosion, Institute for Color Science and Technology, P.O. Box 16765-654, Tehran, Iran
[b] Department of Chemical Engineering, Faculty of Engineering, Golestan University, Aliabad Katoul, Iran

HIGHLIGHTS

- Corrosion inhibition performance of green inhibitor was investigated on mild steel.
- The corrosion inhibition properties were examined by EIS and polarization tests.
- MC and MD simulations revealed the inhibitors adsorption on steel substrate.
- QM computations evidenced the crucial role of reactive sites of inhibitors in their adsorption.

GRAPHICAL ABSTRACT

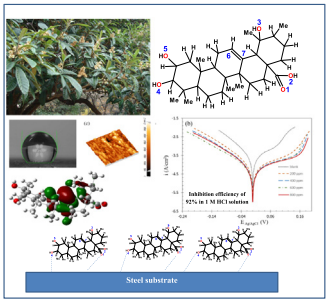

ARTICLE INFO

Article history:
Received 18 December 2018
Received in revised form 15 March 2019
Accepted 2 June 2019
Available online 8 June 2019

Keywords:
Eriobotrya japonica Lindl leaves
HCl solution
Mild steel
Green corrosion inhibition
EIS
Computational method

ABSTRACT

The feasibility of using *Eriobotrya japonica Lindl* (EJL) extract as a green inhibitor towards mild steel corrosion retardation in 1 M HCl solution was evaluated through integrated experimental and computational perspective. By utilizing electrochemical and surface analyses benefits, including EIS, potentiodynamic polarization, SEM, AFM and contact angle test, the protection function of EJL extract was studied. In addition, the EJL extract itself was examined by means of FT-IR and UV–Vis analysis. EIS results revealed the increase in mild steel corrosion resistance in the presence of EJL extract by increasing the extract concentration. The highest resistance was achieved at 800 ppm concentration. A mixed type behavior of EJL extract with dominant anodic dissolution reduction was proved by DC polarization. The lowest current density was obtained at 800 ppm concentration. SEM and AFM images indicated the protective layer growth on steel surface having intact surface morphology and more homogeneity in the presence of inhibitor. Contact angle test results confirmed the steel surface wettability enhancement by addition of EJL extract. The presence of functional groups, which make the inhibitors molecule adsorption possible, was verified by FT-IR and UV–Vis tests results. Furthermore, the computational methods (i.e., quantum mechanics and molecular simulations) evidenced the binding of EJL extract compounds onto steel substrate, affirming the inhibition action of EJL extract.

1. Introduction

Many industrial processes on the metals such as cleaning, pickling, descaling and etc. are conducted by taking advantages of

* Corresponding authors.
E-mail addresses: Gh.Bahlakeh@gu.ac.ir (G. Bahlakeh), ramezanzadeh-bh@icrc.ac.ir, ramezanzadeh@aut.ac.ir (B. Ramezanzadeh).

https://doi.org/10.1016/j.conbuildmat.2019.06.005
0950-0618/

acidic solutions [1–4]. This prevalent method provides severe corrosion attack due to the susceptibility of metals and alloys towards aggressive acidic media, which led to property lost. Employment of organic inhibitors for the acidic solution has been widely considered as a practical protecting approach to diminish the corrosion occurrence [5–9].

The inhibitive behavior of plants extract has been extensively evaluated by many authors and also by this group. Inhibitive performance of *Aloe* extract as a green corrosion inhibitor in the H_2SO_4 solution was proved by utilizing EIS and DC polarization methods by means of which the highest inhibition efficiency was determined about 97% at 30% v/v [10]. In another work, the inhibition function of *Morus Alba Pendula* leave extract (MAPLE) toward carbon steel corrosion mitigation in 1 M HCl solution was examined and by taking advantage of electrochemical analysis 0.4 g/L Maple yielded 93% inhibition efficiency [11]. Satapathy et al. [12] showed that the protection of mild steel in 1 M HCl was strengthened by increasing the concentration of *Justicia Gendarussa* plant extract (JGPE), which acted as a mixed-type inhibitor with concern to the polarization test results. Ji et al. [13] announced the raw banana peel extract as a perfect inhibitor with a 92% efficiency for protection of mild steel in HCl solution. In another study, Zhang et al. declared that chief components of maize gluten meal extract (MGME) are responsible for providing inhibition efficiency (approximately 80%) through which MGME can be regarded as a dependable inhibitor [14]. There are a large number of reports on the application of various plant based green inhibitors for metal corrosion retardation in acidic media. Although they are almost effective but some of them are not cost-effective or show little water solubility. In addition, being available at large scale and showing high inhibition action at lower concentration are other important factors that should be taken into consideration when using a green inhibitor. The extraction efficiency of inhibitor and also the solvent type should be considered. Here, we have tried to suggest an effective green inhibitor with high solubility in water and low price, making it novel over the previously used inhibitors.

In the present study, *Eriobotrya japonica Lindl* (EJL) with common Loquat name is used as a green source of inhibitors for protection of exposed mild steel towards the corrosive acidic solution. Based on the phytochemical analysis, among different parts of EJL, the leaves comprise various organic constituents i.e., triterpenoid acids, flavonoids and sesquiterpene glycosides [15–18] where the major contribution belongs to the triterpenoid acids such as ursolic acid or euscaphic acid [15,18–20]. Expectable inhibitive performance of EJL on the mild steel in the 1 M HCl solution was studied by taking advantages of electrochemical and surface characterization experiments. Furthermore, microscopic level theoretical investigations based on quantum mechanics (QM) and molecular simulations tools were carried out to derive a fundamental understanding concerning the reactivity and adsorption characteristics of green inhibitor.

2. Experimental

2.1. Raw material

Eriobotrya japonica Lindl leaves were gathered from the north of Iran and dried under room temperature condition. To obtain the extract of inhibitor, first 30 g EJL dried powder was added to 1000 ml DI solution and magnetically stirred for 3 h at 70 °C. Thereafter, the obtained extract was filtered completely and to assure entire solvent evaporation it was put in an oven at 60 °C for about 24 h. The chemical structures of ursolic acid and euscaphic acid as the major components of EJL extract are depicted in Fig. 1.

2.2. Sample preparation

The analytical composition (wt.%) of mild steel panels, which were purchased from Foolad Mobarakeh Co. (Iran), was: Fe 93.9%, Mn 1.1%, P 1.2%, Cr 0.7%, Ni 1.7% and Si 1.0%. Prior to electrochemical and surface analyses, 5 cm × 3 cm × 0.2 cm specimens were abraded by 200 to 1200 grit size of emery papers and subsequently, acetone degreasing, DI water rinsing and compressed air drying were executed. Hydrochloric acid (37%) was provided from Merck Co and diluted with DI water in order to prepare 1 M HCl solution. Various concentrations of EJL extract (200, 400, 600, 800 and 1000 ppm) were added to the 1 M HCl solution. Coupons were sealed by the aid of beeswax-colophony mixture (3:1 w/w) and 1 cm^2 area of the surface was left to expose to the inhibited and blank solution.

2.3. Techniques

2.3.1. FT-IR and UV–visible characterization

The possibility of adsorption of EJL extracts molecules on the surface and complex formation was assessed through UV–Visible analysis (Optizen 3220) before and after sample immersion. In addition, the functional groups and chemical bonds present in the extract were characterized by FT-IR (Perkin Elmer) test utilizing KBr powder method in the range of 400–4000 cm^{-1}.

2.3.2. Electrochemical tests

The inhibitive behavior of EJL in the 1 M HCl solution was evaluated by employing EIS and DC polarization. In this regard, common three electrodes set up including saturated calomel reference electrode (SCE), graphite counter electrode and mild steel working electrode was applied. EIS measurements were conducted by using Ivium Compactstat model in the range of 10 kHz–10 mHz frequency range with exertion the sinusoidal wave of 10 mV perturbation at open circuit potential (OCP). The obtained impedance spectra were detailed by using the Zview3.1c software. The DC polarization test was performed in the condition of OCP ± 250 mV potential range and 1 mV sweep rate.

2.3.3. Surface analysis

The impact of extract loaded solution on the surface morphology of mild steel in comparison with the blank solution was investigated by using SEM (XL30 model) analysis. Furthermore, surface degradation in the absence and presence of EJL extract in 1 M HCl solution was studied through surface roughness by using AFM (Dualscope DS 95-200, DME, Denmark). The influence of extract adsorption on the wettability of surface was characterized by contact angle measurement (OCA 15 plus).

3. Computational details

3.1. Quantum mechanics optimization of inhibitor

Fundamental quantum mechanics (QM) explorations were applied for obtaining electronic-level insights into the electronic properties of green inhibitor determining its corrosion inhibition action. Fig. 1 depicts the chemical structure of neutral form of triterpenoid, euscaphic acid and ursolic acid compounds exist in green inhibitor. In order to model the experimental situations (i.e., acidic pH values), the protonated forms of triterpenoid, euscaphic acid and ursolic acid were also taken into consideration. For inhibitor protonation, first all possible protonation sites were recognized including oxygen heteroatoms and double-bonded carbon atoms shown in Fig. 1. Mono-protonated compounds were constructed through protonation of all these potential sites (i.e.,

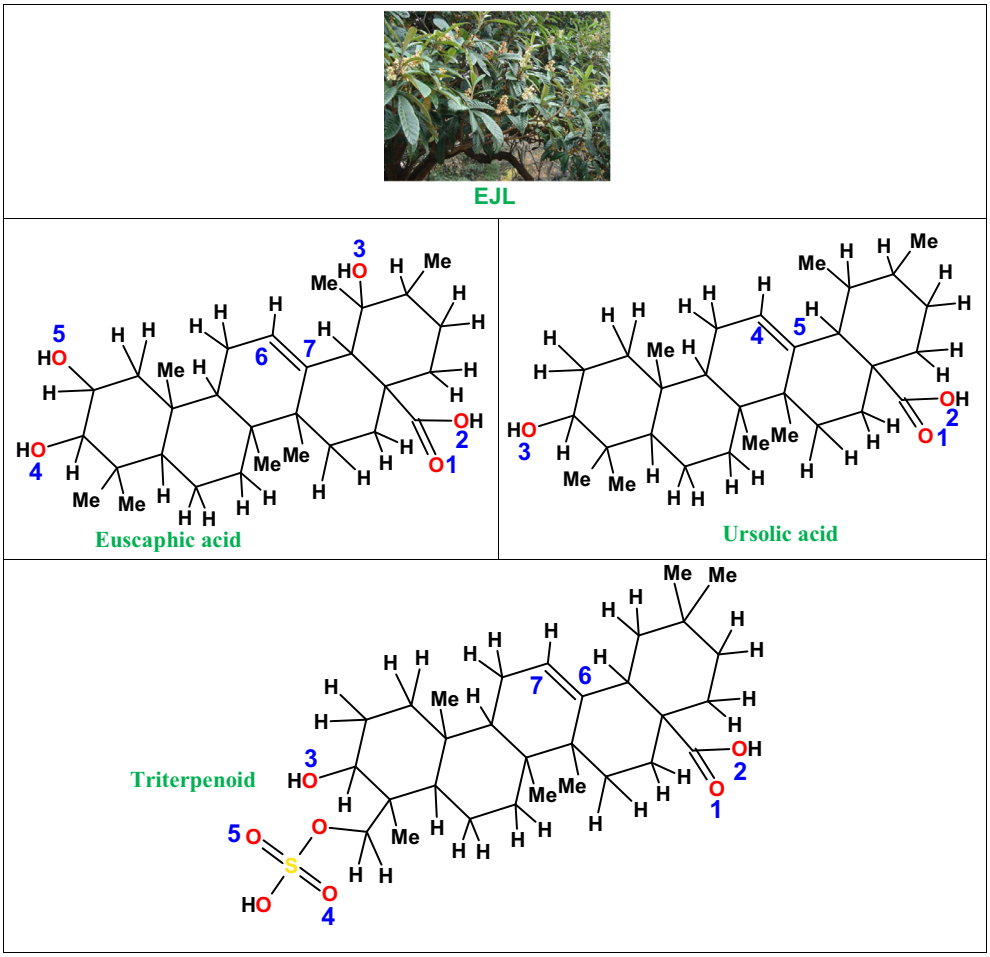

Fig. 1. Chemical structures of neutral form of euscaphic acid, ursolic acid and triterpenoidcompounds exist in green corrosion inhibitor. The oxygen and carbon atoms chosen for protonation are numbered in blue color. For interpretation of color, the reader is referred to the web version of this article.

covalent bonding of a H^+ ion) and then using the QM-optimized geometries the basicity (B) as well as protonation affinity (PA) of each positively-charged compound were determined [21–25] and summarized in Table 1 for triterpenoid, euscaphic acid and ursolic acid species. In the triterpenoid compound protonated from its one of carbon atoms sharing a double bond the highest values of PA and B occurred implying its behavior as the most preferred protonation center. In case of euscaphic acid, it can be seen that even though one of the hydroxyl O atoms possessed slightly higher PA and B compared with the carbonyl O atom of the carboxylic acid moiety, but due to the bond breakage happened upon protonation the carbonyl O site (O4) was identified as the most favorable site subject to protonation under acidic conditions. Additionally, similar to triterpenoid, the backbone C atom involved in double bond in ursolic acid (i.e., C4 atom) served as a site with the greatest affinity for protonation.

The geometries of both neutral and protonated forms of all three compounds of triterpenoid, euscaphic acid and ursolic acid were optimized by means of QM methods in three steps. First, geometry optimization was done with Hartree-Fock (HF) method, which utilized the 6-31G** function [26]. The equilibrated geometries derived from HF calculations were then further optimized by density functional theory, DFT, technique using the B3LYP hybrid exchange–correlation functional for computing the interactions between electrons [27–29]. Within DFT modeling, initially the same basis function of 6-31G** was adopted which was followed

Table 1
The DFT/B3LYP/6-311G** calculated protonation affinity (PA) and basicity (B) (all in kcal/mol) of different oxygen and carbon atoms of protonated compounds.

Atom number	Triterpenoid		Euscaphic acid		Ursolic acid	
	PA	B	PA	B	PA	B
1	248.85	257.10	250.06	257.46	246.65	254.77
2	237.50	249.16	238.52	250.26	239.12	251.44
3	244.13	251.48	243.85	251.97	248.21	255.96
4	230.69	238.57	250.24	258.29	252.38	261.24
5	230.20	238.71	249.54	257.14	245.65	254.00
6	241.00	249.01	248.90	256.52		
7	251.64	259.17	243.90	251.85		

by a larger one, i.e., 6-311G** [30,31]. This successive three-step QM modeling was used to extract fully equilibrated green inhibitor compounds. The SCRF theory in connection with PCM model was applied to implicitly impose the water solvent effects within both HF and DFT calculations [32]. The energy-minimized inhibitor geometries were affirmed by appearance of no imaginary frequencies in output of frequency calculations conducted on the DFT-refined compounds. Gaussian 09 software was used to conduct the QM modeling [33]. Using the equilibrated inhibitor geometries the properties of partial charge, lowest unoccupied molecular orbital (LUMO), highest occupied molecular orbital and (HOMO), the energetic values of E_{HOMO} and E_{LUMO}, the energy gap between frontier orbitals ($E_{LUMO}-E_{HOMO} = \Delta E_{L\text{-}H}$). The inhibitor charges which was subsequently used in classical simulations, were assessed by means of ChelpG method [34]. The value of electron sharing (ΔN) which transferred at the EJL extract/steel interface was analyzed from the electronegativity (χ) and hardness (η) of inhibitor molecules which instead are calculated from the potential of ionization (I) and electron affinity (A). These intrinsic electronic features are defined as [35–38]:

$$\chi = \frac{I + A}{2} = -\frac{E_{HOMO} + E_{LUMO}}{2} \tag{1}$$

$$\eta = \frac{I - A}{2} = \frac{E_{LUMO} - E_{HOMO}}{2} = \frac{1}{2}\Delta E_{L-H} \tag{2}$$

$$\Delta N = \frac{\chi_{Fe} - \chi_{inhibitor}}{2(\eta_{Fe} + \eta_{inhibitor})} = \frac{\Phi_{Fe} - \chi_{inhibitor}}{2\eta_{inhibitor}} \tag{3}$$

To calculate the ΔN value, instead of electronegativity the iron work function $\Phi_{Fe} = 4.82$ was chosen and also its hardness was neglected [36,39,40]. Besides these electronic properties, the electrophilic and nucleophilic behaviors of inhibitors were analyzed through Fukui indices defined according to the expressions of:

$$f^{+}\left(\vec{r}\right) = \rho_{N}\left(\vec{r}\right) - \rho_{N+1}\left(\vec{r}\right) \tag{4}$$

$$f^{-}\left(\vec{r}\right) = \rho_{N}\left(\vec{r}\right) - \rho_{N-1}\left(\vec{r}\right) \tag{5}$$

The nucleophilic attack was shown by $f^{+}\left(\vec{r}\right)$ and the $f^{-}(\vec{r})$ denotes the electrophilic attack. Also, the $\rho_{N+1}\left(\vec{r}\right)$, $\rho_{N}\left(\vec{r}\right)$ and $\rho_{N-1}\left(\vec{r}\right)$ terms are demonstrative of the density in an negatively-charged, neutrally-charged and positively-charged molecule, respectively. These properties were also determined using DFT modeling by DMol^3 code applying the GGA/PBE scheme and basis function of DNP for the analysis of electronic interactions [41].

3.2. Molecular simulations

To examine the adsorption affinity of inhibitor compounds on metal substrate the classical molecular simulations were used. To this purpose, using the iron unit cell an appropriate crystalline Fe (1 1 0) surface was first prepared with a thickness of 1.5 nm and a 14×14 periodic replication. The crystallographic facet of (1 1 0) in iron unit cell is a high packed and the lowest energy surface (i.e., the most thermodynamically stable) among various iron surfaces and has been frequently adopted in literature to be representative of the steel adsorbent [21,37,42–48]. By putting a 3 nm vacuum space the cleaved two-dimensional surface was converted to a three-dimensional slab model. This Fe (1 1 0) cell and minimum energy triterpenoid, euscaphic acid and ursolic acid compounds extracted from the last step of DFT modeling were used as input for Monte Carlo (MC) simulations [49]. A convergence value of 1×10^{-4} kcal.mol^{-1} for energy parameter and 5×10^{-3} kcal.mol^{-1}.Å^{-1} for force was considered. Also, the convergence of displacement was monitored by 5×10^{-5} Å. Similar to QM computations, classical molecular dynamics (MD) simulation was done in liquid-phase medium through explicitly incorporation of solvent molecules. For this purpose, 600 molecules of water were put inside a layer-type cell constructed at 1 g/cm^3. This layer was added to the last lowest energy configuration resulted from MC simulations. Afterwards, the constructed cells containing water molecules, inhibitor and iron surface were optimized by means of Smart minimizer for 20,000 steps with convergence levels of 1×10^{-4} kcal/mol, 5×10^{-3} kcal/(mol.Å) and 5×10^{-5} Å selected for energy, force and displacement, respectively. Subsequently, MD computations were conducted on optimized cells under NVT ensemble situations for 1 ns using 0.25 fs time step and temperature of 298 K. The optimization and MD simulations were carried out employing Forcite module in Materials studio software.

Within optimization and MC as well as MD simulations, COMPASS force field [50,51] was employed to represent the potential energy as it has been successfully applied in previous theoretical evaluations of inhibitor adsorption on the metallic substrates [21,37,42–45,52]. The partial charges of triterpenoid, euscaphic acid and ursolic acid species were taken from DFT calculations and the electrostatic interactions were described by Ewald scheme while the van der Waals interactions of EJL extract molecules were characterized applying atom-based cutoff approach with 12.5 Å cutoff radius. To integrate the Newton equation within MD simulations the velocity Verlet integrator was adopted [53]. Furthermore, the temperature was controlled via thermostat of Nose-Hoover [54,55]. All surface atoms were frozen within simulations.

4. Results and discussion

4.1. Characterization of EJL

The presence of some major functional groups in the EJL chemical structure, which establish the adsorption of inhibitor molecule on metal surface and protective film formation, was studied by FT-IR analysis. FT-IR plot is displayed in Fig. 2(a). Due to the characterization of adsorption peaks in the literature [11,56–58] and the peaks appeared in the spectrum of Fig. 2(a), the peaks in the range of 600–1000 cm^{-1} can be attributed to the bending of C—H bands present in the alkenes structure. The stretching vibration of alcohol C=O bands can be assigned to the peak observed at 1036.39 cm^{-1}. The peak at 1263 cm^{-1} corresponds to the C=O stretching and/or O—H deformation of carboxylic groups. The peak noticed at 1409.74 cm^{-1} is related to the bending vibration of carboxylic O—H groups and/or stretching of alcohol C=O bands or illustrates the aliphatic C–H deformation. On the other hand, two absorption peaks at 1036.39 and 1409.74 cm^{-1} can be the indication of C—C stretching and bending modes, respectively. The absorption peak at 1615.60 appoints to the stretching of carbonyl groups that can be seen in the form of ester, carboxylic acid or aldehyde. Aliphatic C—H stretching modes are demonstrated at 2924.22 cm^{-1} and eventually the stretching modes of hydroxyl group appear at 3424.31 cm^{-1}.

These determined functional groups can be clearly observed in the ursolic and euscaphic acid.

The possibility of complex formation between the inhibitors and Fe^{2+} cations was analyzed by running UV–visible analysis before and after steel coupons subjection to the inhibited solution. As it can be seen from Fig. 2(b), the intensity of the peaks in the range of 250–320 nm, which indicates the presence of O—H and COOH functional groups (n-π^*) in the EJL chemicals [56,59], is

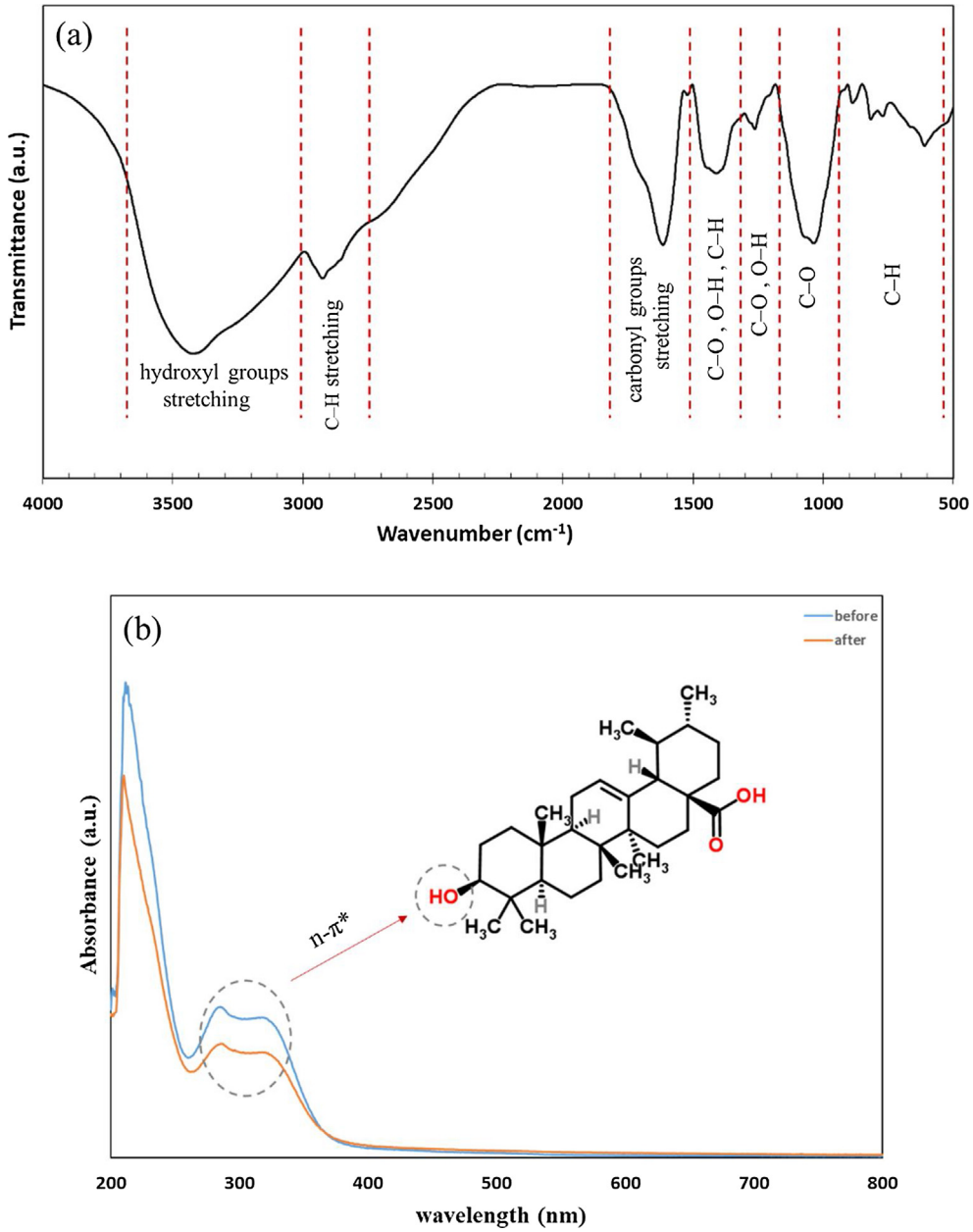

Fig. 2. (a) FT-IR analysis of EJL extract, (b) UV–Vis curves of inhibited solution before and after steel coupon dipping.

decreased after dipping. This drop shows the consumption of functional groups in the complex formation with metallic cations through sharing their free electrons with unfilled orbitals of Fe^{2+}. Thus, it can be deduced that the inhibitors molecules possibly interacted with mild steel surface.

4.2. Electrochemical measurements

Protective behavior of various concentrations of EJL extract for mild steel surface towards 1 M HCl solution was evaluated by applying electrochemical impedance spectroscopy and potentiodynamic polarization experiments. Nyquist and Bode spectra from EIS measurements are illustrated in Fig. 3 and Fig. S1, respectively. With concerning the shape of Nyquist diagrams which appear in a single semicircular form, it can be concluded that the response of the system (substrate/solution interface) must pertain to the charge transfer. Moreover, no noticeable change in the shape of Nyquist spectra meanwhile increasing the concentration of inhibitor can be seen. This can validate that the corrosion occurrence is under charge transfer control and no mechanism change happens. However, the lack of perfect homogeneity of the surface results in no accurate semicircle figure of spectra. As the inhibitor concentration raised the increase of Nyquist diagrams diameter besides the increase of low frequency impedance ($|Z|_{0.01Hz}$) values as well as phase angle at high frequency (θ_{10kHz}) occurred, indicating the more mitigation of corrosion reactions through blocking the active sites which stems from approaching and absorption of inhibitors' molecules on the surface of steel plate. Due to the unchangeable behavior of the blank solution during all immersion times, the typical spectrum of the blank solution after 30 h is depicted in all plots.

Thus, according to the plots, an electrical equivalent circuit with one-time constant was suggested (Fig. 3) to analyze the impedance spectra and take out the electrochemical parameters in details. The proposed circuit consists of R_s, R_{ct} and CPE_{dl}, which are assigned to

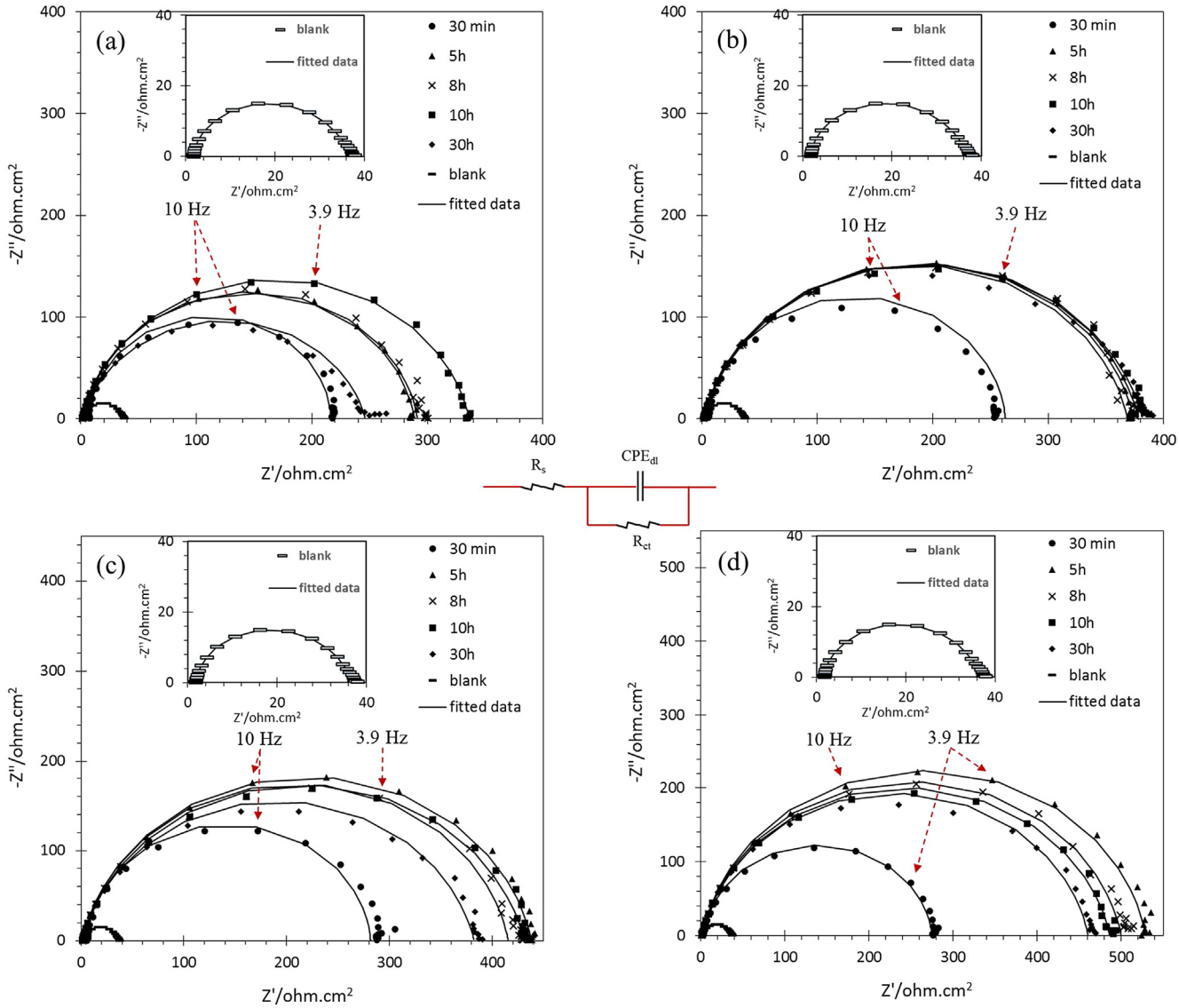

Fig. 3. Nyquist spectra of mild steel panels immersed in the solution test with (a) 200 ppm, (b) 400 ppm, (c) 600 ppm and (d) 800 ppm of EJL extract in comparison with blank solution.

the solution resistance, charge transfer resistance and constant phase element of double layer, respectively. The extracted electrochemical parameters are listed in Table 2. Calculation of double layer capacitance was done by using Eq. (6):

$$C_{dl} = \left(Y_0.R_{ct}^{1-n}\right)^{1/n} \tag{6}$$

where Y_0 and n describe the CPE admittance and homogeneity degree, respectively. The efficiency of inhibition was determined through Eq. (7):

$$\eta\% = 100\left(1 - \left(\frac{R_{ct.0}}{R_{ct.i}}\right)\right) \tag{7}$$

where $R_{ct,i}$ and $R_{ct,0}$ define the charge transfer resistance in the presence and absence of EJL extract, respectively. In other words the Eq. (7) explains the surface coverage θ (η/100).

Concerning the R_{ct} trends reported in Table 2, the increment of EJL concentration led to more adsorption of inhibitors on the surface and strengthening the interface condition against aggressive electrolyte. In this regard, the inhibition efficiency, obtained through blocking the active anodic and/or cathodic area reveals the successful contribution of organic constituents presents in the EJL extract. 800 ppm concentration shows the highest resistance among all added concentrations. The adsorption of inhibitor molecules led to the water molecules replacement with organic molecules at metal/electrolyte interface. Hence, keeping away the water molecules from the surface by inhibitor adsorption results in the reduction of dielectric constant and the increase of double layer distance. Consequently, the capacitance of double layer getting lower by increasing the inhibitor adsorption and resistant film production. The height of phase angle also indicates the capacitive behavior of the interface in the presence of inhibitors in comparison with uninhibited test solution.

By approaching the inhibitors compounds to the surface of mild steel, probably the oxygenated functional groups of EJL can share their lone pair of electrons with the vacant d orbitals of Fe and form insoluble complexes on the surface which cover the susceptible zones and hinder the corrosion reactions. Additionally, organic species can be protonated in acidic solutions and adsorb on the surface through electrostatic attraction. Therefore, both

Table 2
Extracted electrochemical parameters from EIS data during 30 h subjection to 1 M HCl solution.

EJL Concentration	Immersion time (h)	Y_0[a] ($\mu\Omega^{-1}$ cm^{-2} s^n)	n[b]	R_{ct}[c] (Ω cm^2)	C_{dl}[d] (μF cm^{-2})	η (%)
0 ppm	0.5	142	0.93	38.4	109.1	–
	5	594	0.92	35.5	437.5	–
	8	929	0.90	35.2	660.4	–
	10	1200	0.92	35.1	912.4	–
	30	3090	0.91	33.6	2475.7	–
200 ppm	0.5	62	0.97	208.8	63.2	81.6
	5	112	0.90	299.1	78.7	88.1
	8	124	0.89	305.4	86.8	88.4
	10	140	0.88	311.5	91.3	88.7
	30	206	0.86	245.2	120.6	86.2
400 ppm	0.5	63	0.94	248.4	61.3	84.5
	5	101	0.87	338.9	60.7	89.5
	8	105	0.86	343.6	62.8	89.7
	10	101	0.86	377.0	62.9	90.6
	30	112	0.85	356.1	67.6	90.5
600 ppm	0.5	55	0.94	292.0	43.1	86.8
	5	77	0.90	435.6	50.1	91.8
	8	77	0.90	413.9	50.7	91.4
	10	85	0.87	414.7	51.6	91.5
	30	98	0.87	364.0	62.5	90.7
800 ppm	0.5	55	0.93	279.2	49.9	86.2
	5	80	0.88	495.6	51.0	92.8
	8	86	0.87	487.4	52.4	92.7
	10	87	0.87	484.8	52.5	92.7
	30	90	0.88	459.1	51.6	92.6

[a] The standard deviation range for Y_0 values was 4.2%–7.3%.
[b] The standard deviation range for n values was 2.2%–10.6%.
[c] The standard deviation range for R_{ct} values was 1.2%–9.7%.
[d] The standard deviation range for C_{dl} values was 3.5%–11.8%.

chemisorption and physisorption are the possible inhibiting mechanism. The most inhibition efficiency was achieved at 800 ppm concentration of EJL extract which is in the range of 85–95% inhibition efficiency [13,60]. As a result, it can be pronounced as an effective and applicable green inhibitor for mild steel protection in the acidic solution.

In order to determine the adsorption mode of EJL extract, the adsorption of extract on the surface was studied by utilizing various isotherms. Among the studied isotherms, Langmuir isotherm was exhibited the best fit for extracting the inhibitor adsorption on the mild steel surface (Fig. 4). This isotherm defines the correlation between the surface coverage and inhibitor concentration through following equation:

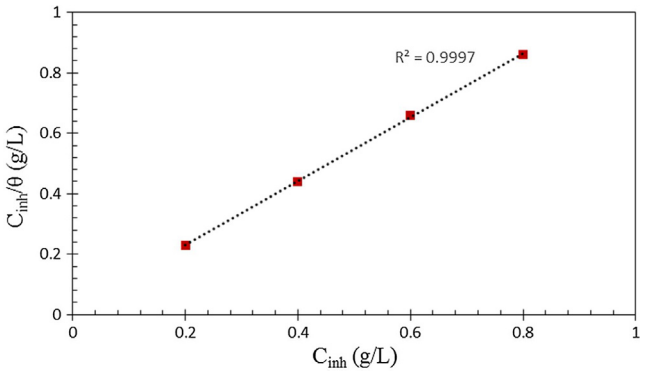

Fig. 4. Fitted Langmuir adsorption isotherm on the derived impedance data of mild steel panels after 30 h dipping in the 1 M HCl solution.

$$\frac{C_{inh}}{\theta} = \frac{1}{K_{ads}} + C_{inh} \quad (8)$$

where C_{inh}, θ and K_{ads} are corresponded to the concentration of EJL extract, degree of surface coverage and adsorption equilibrium constant, respectively. From Fig. 4, the spectrum of C_{inh}/θ as a function of C_{inh} was fitted with straight line with regression coefficient of 0.9997, which is perfectly close to 1, confirming that the adsorption procedure obeys Langmuir isotherm [10,11].

The effect of EJL extract on the anodic or cathodic reactions was analyzed more accurately by conducting potentiodynamic polarization test. Fig. 5 shows the polarization curves after 30 h immersion in the inhibitor containing and blank solutions. In addition, for a better comparison, all plots were shifted to the zero potential. By utilizing Tafel extrapolation method, the polarization parameters including E_{corr}, i_{corr}, β_a and β_c are measured and reported in Table 3. As it can be seen, addition of extract regardless of its concentration reduces the anodic and cathodic current densities noticeably and dislocates the corrosion potential to the more negative values. The amount of the most E_{corr} displacement is not notable to discuss about the inhibitor type [61]. Besides, both anodic and cathodic slopes kept almost unchanged, indicating that no mechanism changing in the presence of EJL extract occurs. However, the variation of anodic slopes is more noticeable which implies the chemisorption behavior on the anodic zones whereas the inhibitive performance on the cathodic zones is in the physisorption with no hydrogen evolution reaction change. The lowest corrosion rate was obtained at concentration of 800 ppm.

4.3. Surface characterization

SEM images of samples after 30 h immersion in the blank acidic and inhibitor containing solutions are depicted in Fig. 6. It is clear

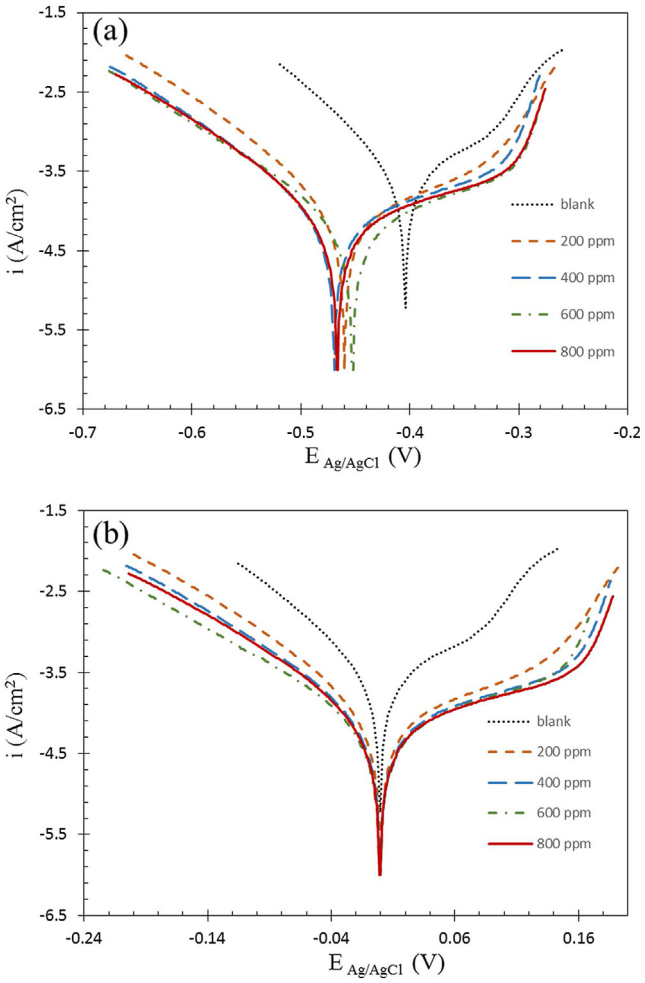

Fig. 5. (a) Polarization curves of mild steel plates in the blank and inhibited solution test after 30 h immersion and (b) all plots were shifted to 0 potential.

from the pictures that the most severe corrosion attack was happened in the blank solution and produced corrosion products which agglomerated on the surface. In contrast, the surface morphology of the solution containing 800 ppm EJL extract remains almost intact. Actually, the adsorption of inhibitors molecule on the surface and production of inhibitive layer block the active corrosion area and prevents the access of corrosive species to the surface. Thus, the anodic dissolution happens at the lowest rate and the surface conditions were kept unchanged.

Homogeneity and roughness of the mild steel surface after 30 h being in the 1 M HCl solution without and with 800 ppm of EJL extract were characterized by employing AFM (Fig. 7). The samples as received were used as reference. Extreme corrosion occurrence produces rough and destroyed surface for the samples in the blank solution while the smooth and homogenize surface is observed for the 800 ppm loaded solution and the roughness is remarkably decreased S_y for blank and 800 ppm loaded solutions is 1750 and 459, respectively. Adsorption of inhibitors on the surface and limiting the corrosion happening preserved the surface undamaged, which is in consistency with electrochemical results.

Fig. S2 illustrates the side view of the water droplet and corresponded to the measured contact angle of the samples immersed in the 1 M HCl in the absence and presence of 800 ppm of EJL extract. Organic compounds with hydrophilic nature must increase the angle between the water droplet and interface. Due to the pictures, more contact angle is obtained which clearly confirms the adsorption and development of organic compounds on the substrate in the form of protective film (blank solution 59° and 800 ppm loaded solution test 100°).

4.4. Molecular simulation

Atomic-scale simulations (MC and MD) were done to examine the adsorption of EJL extract substances with respect to the steel adsorbent. Fig. 8 demonstrates the top views of ultimate cells containing lowest energy structures of both forms of EJL extract species (neutral and mono-protonated) including triterpenoid, euscaphic acid and ursolic acid obtained from MC simulations. It is noted from the visualized snapshots that the neutrally-charged and positively-charged compounds stabilized over the iron surface with flat alignment of their molecular backbone. Such a computational observation suggests the tendency of selected materials to adsorb onto iron surface. Different energetic outputs related to these snapshots are provided in Table 4 for each inhibitor. It is seen from the summarized data that the energies of triterpenoid, euscaphic acid and ursolic acid molecules adhered to surface are negative, an observation quantitatively illustrating the adsorption capacity of chosen inhibiting materials over the steel surface.

The side views of equilibrated triterpenoid, euscaphic acid and ursolic acid configurations, generated after 1 ns MD simulations are gathered in Fig. 9. Inspection of these structures indicates that corrosion inhibitors are able to attach onto crystalline surface (1 1 0) of pure iron metal even in humid environments. The adsorption of triterpenoid, euscaphic acid and ursolic acid was further assessed by the analysis of adsorption energy [52,62]. The computed adsorption energies amount to −211.84, −176.33 and −153.85 kcal/mol for neutral and −203.03, −154.80 and −155.45 kcal/mol for protonated triterpenoid, euscaphic acid and ursolic acid compounds, respectively. Predicted energies of negative magnitude for EJL extract compounds adsorption are another indication of their capability of binding to iron surface. This instead exhibits the formation of a corrosion-resistant layer. These theoretical findings support the corrosion protection features of green inhibitor observed in our experiment.

4.5. Quantum mechanics results

Ab initio computations were conducted for EJL extract molecules to derive electronic-level details concerning the adhesion mechanism and local reactivity of inhibitor molecules. From an

Table 3
Detailed electrochemical parameters from DC polarization of mild steel coupons immersed in the inhibitor containing and blank solutions after 30 h.

Sample	i_{corr} (μA/cm^2)	E_{corr} (V)	b_a (mV/decade)	-b_c (mV/decade)
Blank	31.2 ± 0.3	−0.4025 ± 0.014	0.015 ± 0.002	0.013 ± 0.001
200 ppm	11.5 ± 0.8	−0.4578 ± 0.020	0.019 ± 0.004	0.018 ± 0.006
400 ppm	10.2 ± 0.6	−0.4667 ± 0.031	0.029 ± 0.006	0.022 ± 0.004
600 ppm	7.4 ± 0.4	−0.4506 ± 0.024	0.022 ± 0.007	0.019 ± 0.003
800 ppm	6.9 ± 0.2	−0.4643 ± 0.017	0.018 ± 0.001	0.017 ± 0.003

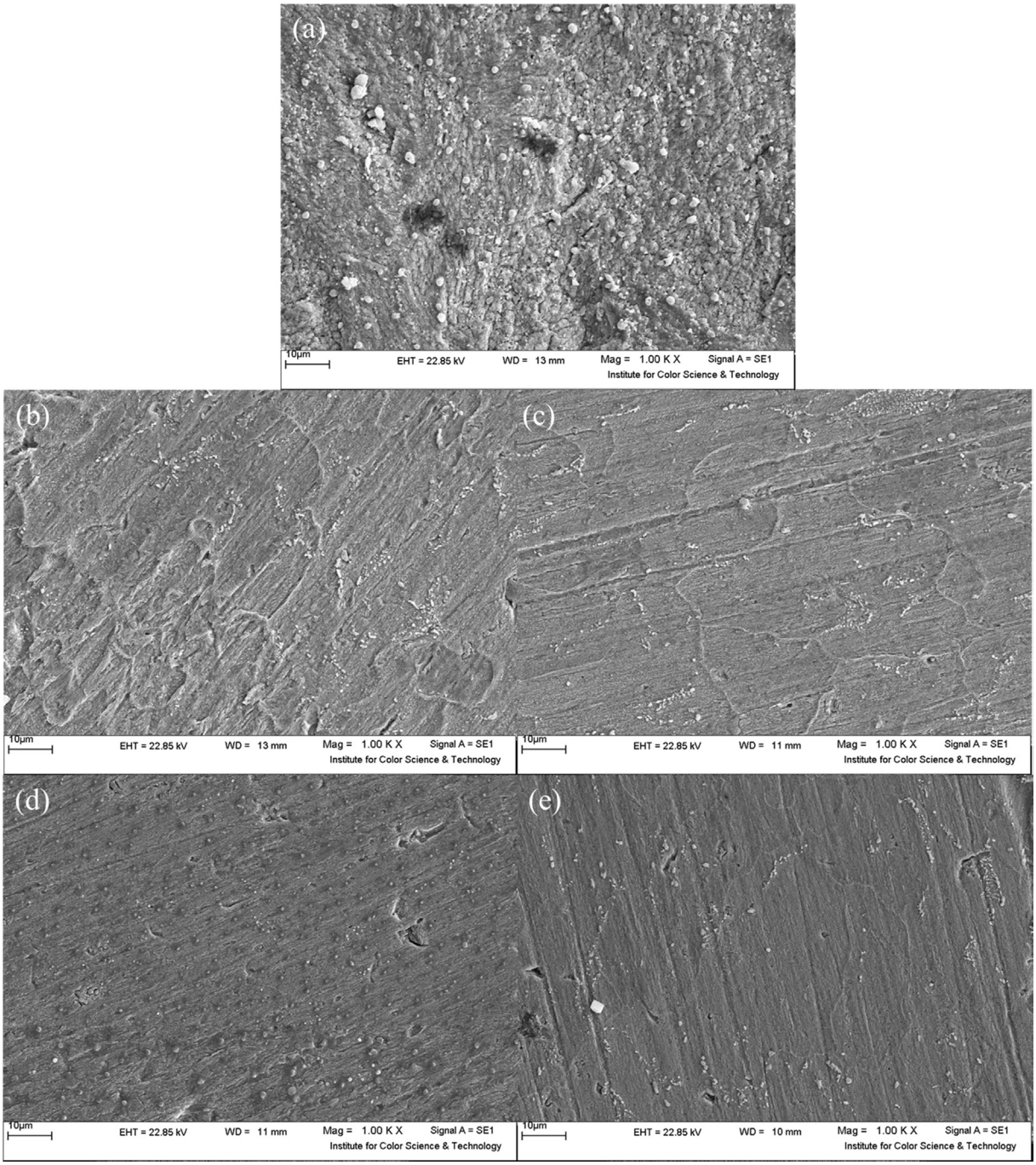

Fig. 6. Surface morphology of mild steel panels after 30 h immersion in the 1 M HCl in the absence (a) and presence of (b) 200 ppm, (c) 400 ppm, (d) 600 ppm and (e) 800 ppm of EJL extract.

electronic scale viewpoint it is believed that the adhesion of corrosion inhibiting materials on a metallic adsorbent takes place through the interfacial donor–acceptor interactions between inhibiting molecule and metal surface [35,38,63–65]. In this adhesion mechanism, the aromatic cycles, heteroatoms (e.g., N and O) and double bonds in inhibitor which are electron-rich centers donate their electrons to electron-poor sites of metal surface. The capability of an inhibitor molecule to give and take electrons is determined by its frontier orbitals, that is, HOMO and LUMO, respectively.

Fig. 10 illustrates the energy-minimized geometries of euscaphic acid, triterpenoid and ursolic acid species extracted from DFT modeling. The graphical molecular orbital results related to these optimized inhibitors are displayed in Figs. 11 and S3 for neutral and protonated molecules. It is noted from Fig. 11 that the HOMO of neutral triterpenoid distributed mostly on the C=C double bond and also its neighboring carbon atoms implying the greatest electron supplying ability of this double bond. The LUMO of this molecule on the other side emerged on the carbon atoms of this region and also on the carboxylic acid moiety, an observation

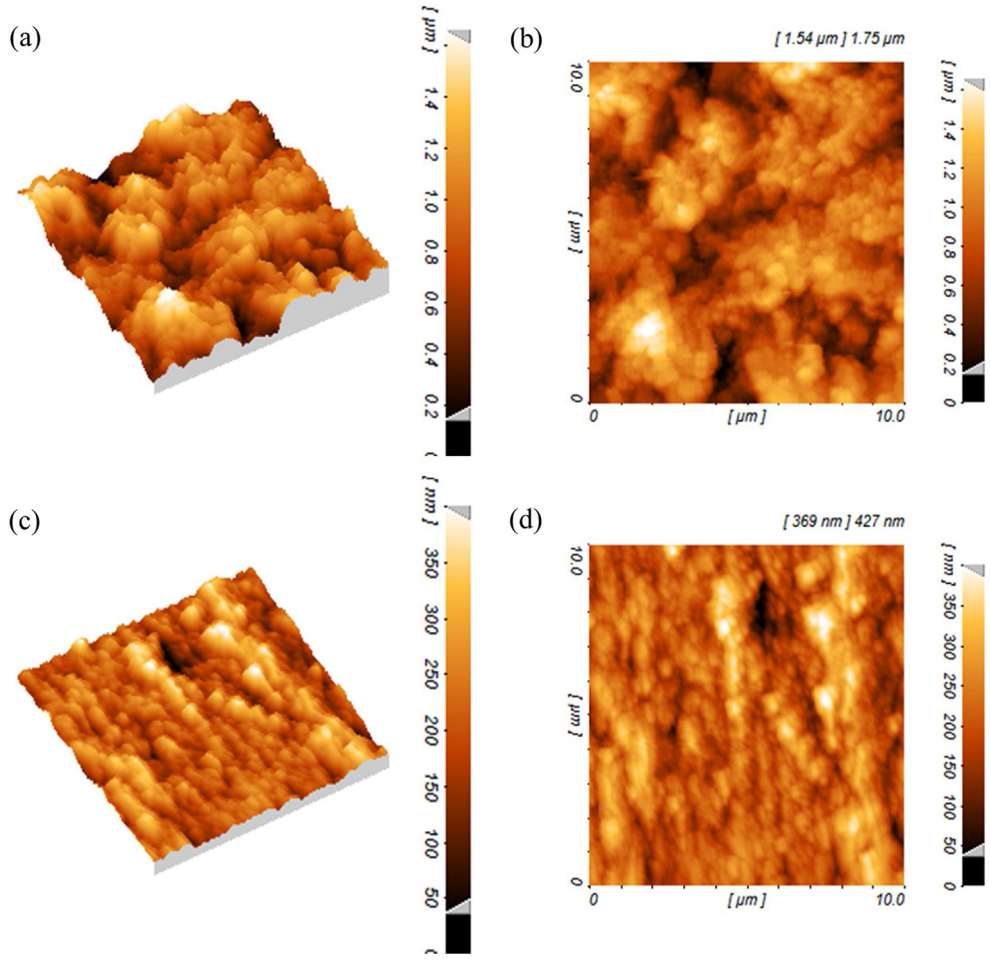

Fig. 7. 2D and 3D AFM images of the mild steel surface dipped in the 1 M HCl solution without (a), (b) and with 800 ppm EJL extract (c), (d).

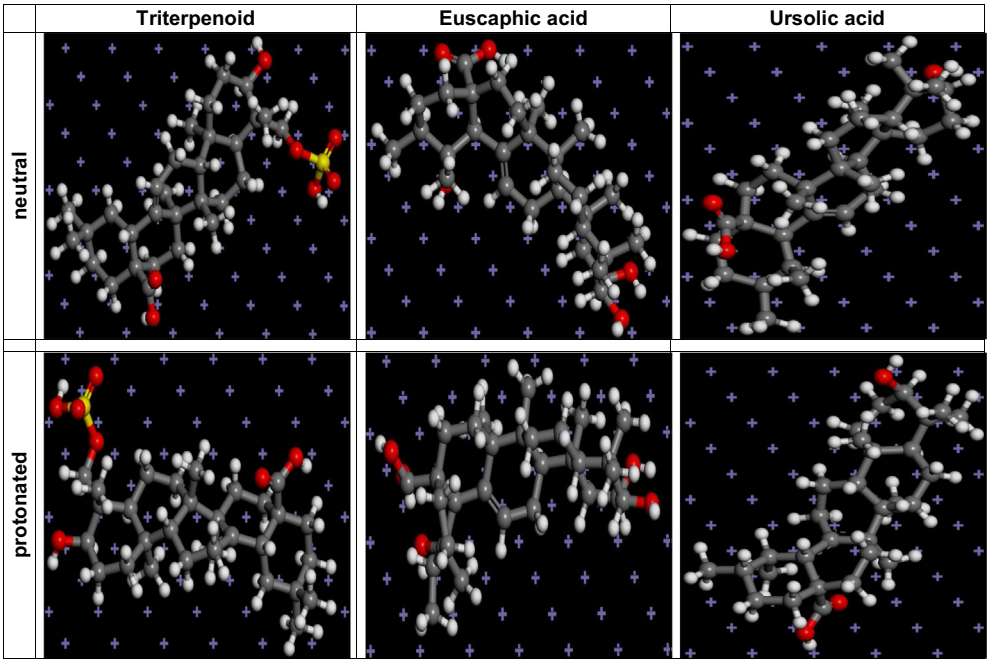

Fig. 8. The final snapshots of neutral and protonated triterpenoid, euscaphic acid, and ursolic acid compounds over Fe (1 1 0) surface obtained from Monte Carlo simulations.

Table 4
The energetic outputs and descriptors (all in kcal/mol) obtained from Monte Carlo simulations of neutral and protonated triterpenoid, euscaphic acid, and ursolic acid compounds over the Fe (1 1 0) substrate.

Molecule	Total energy	Adsorption energy	Rigid adsorption energy	Deformation energy	dE_{ads}/dN_i
Neutral					
Triterpenoid	−452.69	−231.96	−213.56	−18.39	−231.96
Euscaphic acid	−190.47	−187.90	−183.85	−4.05	−187.90
Ursolic acid	−101.93	−164.02	−162.65	−1.37	−164.02
Protonated					
Triterpenoid	−407.66	−259.82	−225.95	−33.87	−259.82
Euscaphic acid	−171.10	−223.17	−196.32	−26.85	−223.17
Ursolic acid	−63.64	−186.69	−170.48	−16.21	−186.69

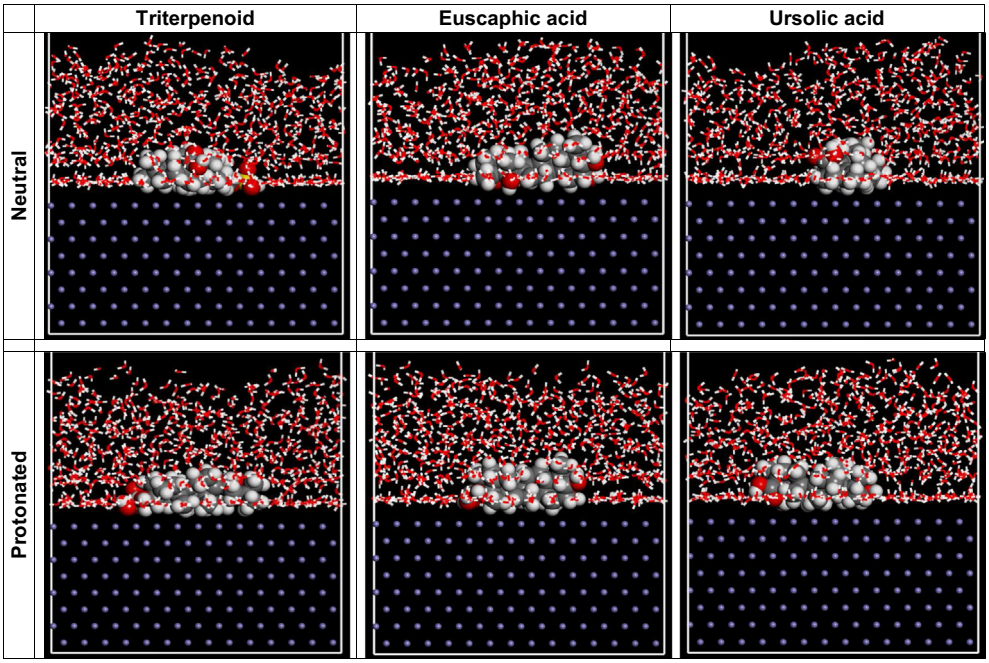

Fig. 9. The final snapshots of neutral and protonated triterpenoid, euscaphic acid, and ursolic acid compounds over Fe (1 1 0) surface obtained from molecular dynamics simulations.

proposing the preference of these reactive sites for accepting electrons. Similarly, it can be observed in case of neutral acidic compounds (i.e., euscaphic acid and ursolic acid) that the HOMO explicitly appeared on single double bond between backbone carbon atoms and also slightly extended to its neighboring atoms. Such a distribution of HOMO evidences the reactivity and the highest chance of electron transfer from the double bond to empty orbitals of iron atoms. Additionally, as shown the LUMO of the acidic species principally located on the carboxylic acid functionality, which highlights the involvement of this fragment in inhibitor/metal donor-acceptor interactions by acceptance of electrons from surface centers owning filled d orbitals. Following the HOMO/LUMO pictures of positively-charged molecules provided in Fig. S3, it is seen that the frontier orbitals of protonated euscaphic acid is nearly the same as those of neutral one. However, protonation noticeably affected the distribution of frontier orbitals in the protonated triterpenoid and ursolic acid. It is visible that in both of these molecules one of the hydroxyl fragments and its neighboring ring acted as major HOMO regions and thus charge sharing towards the unfilled metal orbitals could occur from these active sites. On the other side, the protonated atom served as a reactive center for LUMO declaring its electron accepting tendency.

The electron donation and accepting propensities of inhibitors were quantitatively checked by the molecular orbital energies (E_{HOMO}, E_{LUMO} and ΔE_{L-H}), fraction of migrated electrons (ΔN) and other intrinsic parameters including electron affinity, ionization potential, electronegativity and hardness. All these quantum chemical features are collected in Table 5 for neutral and protonated molecules.

According to literature, the frontier HOMO of less negative energy is able to transfer more electronic charges and a LUMO of more negative eigenvalue can receive more charges. As a consequence, an inhibitor with a lower energetic gap occurred between its HOMO and LUMO could effectively contribute in donor-acceptor interactions with metallic adsorbent [62]. As presented in Table 5, the neutral triterpenoid possessed the lowest LUMO energy and HOMO/LUMO energetic difference clarifying its strongest donor-acceptor interactions and thus the triterpenoid could play a critical role in adsorption and subsequent corrosion protection effect of green inhibitor. This quantum chemical observation is in accordance with the calculated highest adsorption energy of triterpenoid molecule using MC and MD simulations. Moreover, it is noted that the fraction of electrons transferred is close to zero in case of protonated euscaphic acid and is negative for protonated

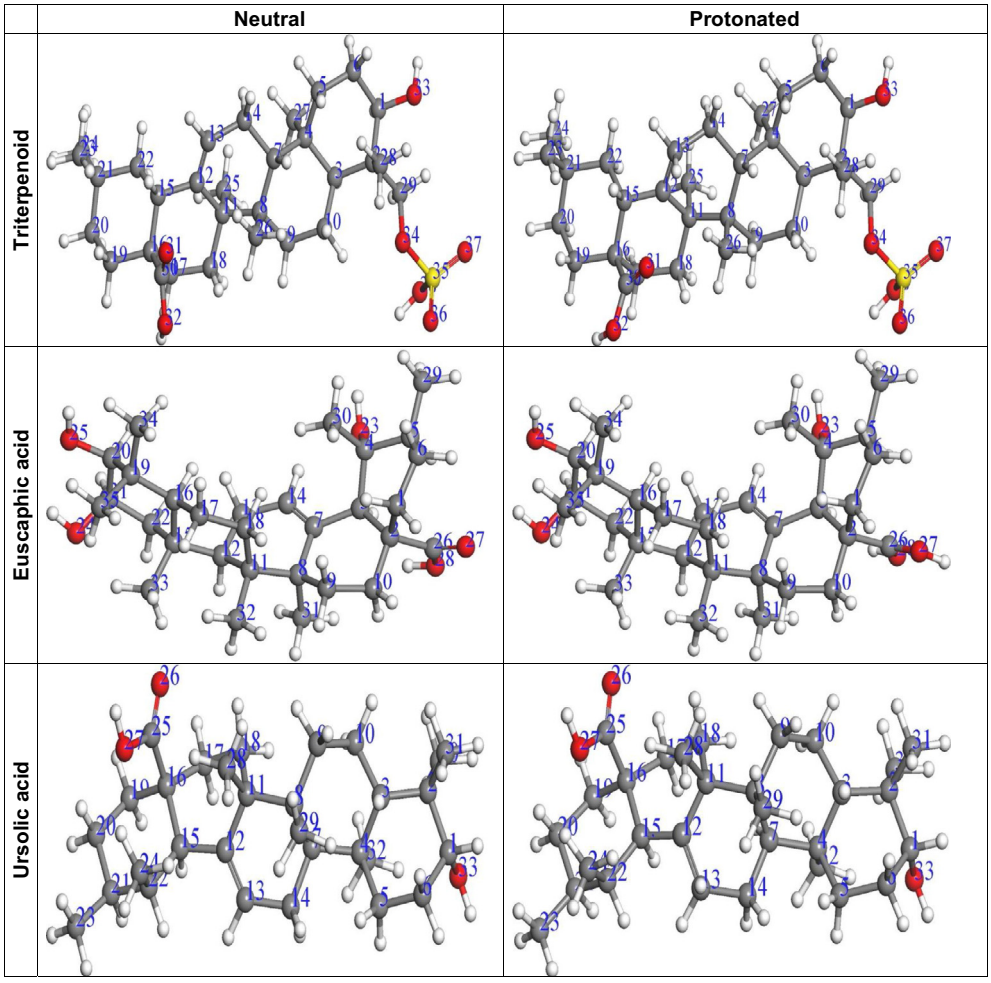

Fig. 10. The B3LYP/6-311G** optimized geometry of neutral and protonated triterpenoid, euscaphic acid, and ursolic acid compounds.

triterpenoid and ursolic acid substances, an evident observation displaying the electron accepting preference of protonated inhibiting molecules.

The local reactive sites of green corrosion inhibitor compounds were further examined by Fukui indices. These indices exhibit the electrophilicity and nucleophilicity. Figs. 12 and S4 indicate the atom-condensed Fukui functions, which include f^- representative of electrophilic character and f^+ demonstrative of nucleophilic attacks of EJL extract molecules, i.e., euscaphic acid, triterpenoid and ursolic acid species. The respective values of these two functions are summarized in Tables 6 and S1.

The graphical results apparently declare that the Fukui indices in neutral triterpenoid that the electrophilic attacks emerged chiefly over carbon atoms in C=C double bond and slightly on the neighboring C atoms. This observation can be confirmed by the data tabulated in Table 6 as the f^- function on C12 and C13 atoms possessed significant values of 0.128 and 0.176, respectively. Accordingly, identical to HOMO results of neutral triterpenoid the carbon atoms forming the double bond could give their electrons whenever they were attacked by an electrophile. On the other hand, the nucleophilic type attacks of neutral triterpenoid are noted to occur on carboxylic acid moiety which is also apparent from the large f^+ function values of 0.200, 0.218 and 0.121 related to C30, O31 and O32 atoms, respectively. Therefore, the COOH fragment of neutral triterpenoid served as a reactive site with nucleophilic nature and thus could accept charges when exposed to a nucleophilic site. In case of neutral acidic corrosion inhibiting species, i.e., euscaphic acid and ursolic acid, the carbon atoms sharing the double bond behaved as major active centers with electrophilic attacks. The values of f^- function in Table 6 for these acidic molecules further highlight the preferred electrophilic interactions of double bond as the C7 and C14 atoms in euscaphic acid and C12 and C13 atoms in ursolic acid owned considerably large values as compared with the other atoms. It is inferred from these graphical and quantitative results that the double bond in acidic compounds contributes in donor–acceptor interaction through providing electrons upon attacking by an electrophile like empty d orbitals of surface iron atoms. Furthermore, as shown in Fig. 12 and Table 6, the nucleophilic behavior of both neutral acids appeared on the carboxylic acid functionality, revealing the fact that this fragment tends to accept electrons which is in line with corresponding LUMO results. For the case of protonated molecules, the Fig. S4 and Table S1 clearly prove that the electrophilic and nucleophilic behaviors are similar to their corresponding HOMO and LUMO results. The hydroxyl oxygen in protonated triterpenoid as well as ursolic acid and the ring double bond in euscaphic acid showed electrophilic attacks. In addition, in all three molecules, the nucleophilic attacks are noted to take place over the protonated region which clarifies the receiving of electrons using this region of inhibitors when exposed to a nucleophile.

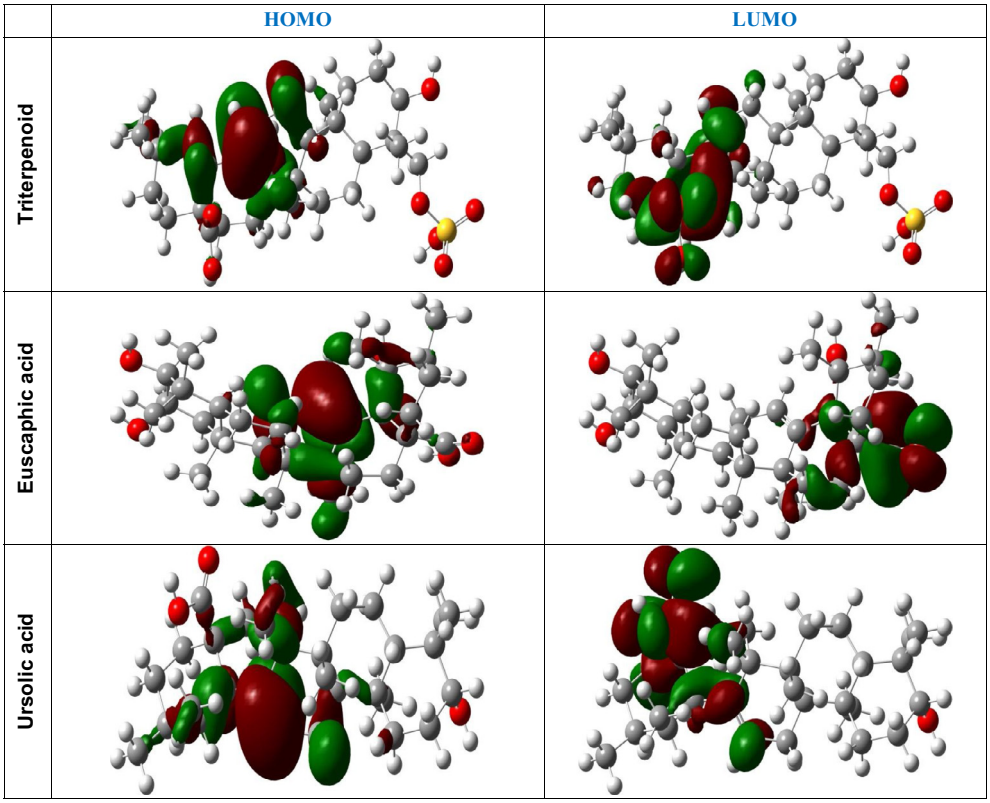

Fig. 11. The HOMO and LUMO of neutral triterpenoid, euscaphic acid, and ursolic acid compounds.

Table 5
The HOMO and LUMO energies (eV), E_{LUMO} - E_{HOMO} energy gap ($\Delta E_{L\text{-}H}$), electron affinity (A), ionization potential (I), electronegativity (χ), hardness (η), and fraction of electrons transferred (ΔN) for neutral and protonated triterpenoid, euscaphic acid, and ursolic acid compounds.

Molecule	E_{HOMO}	E_{LUMO}	$\Delta E_{L\text{-}H}$	A	I	χ	η	ΔN
Neutral								
Triterpenoid	−6.235	−0.169	6.066	0.169	6.235	3.202	3.033	0.2667
Euscaphic acid	−6.206	−0.063	6.143	0.063	6.206	3.135	3.072	0.2742
Ursolic acid	−6.210	−0.103	6.107	0.103	6.210	3.157	3.054	0.2722
Protonated								
Triterpenoid	−7.542	−3.742	3.800	3.742	7.542	5.642	1.900	−0.2163
Euscaphic acid	−6.462	−2.543	3.919	2.543	6.462	4.503	1.960	0.0809
Ursolic acid	−7.247	−3.839	3.408	3.839	7.247	5.543	1.704	−0.2121

Table 6
The Fukui indices of electrophilic and nucleophilic behaviors of neutral triterpenoid, euscaphic acid, and ursolic acid compounds.

Triterpenoid			Euscaphic acid			Ursolic acid		
Atom	f^-	f^+	Atom	f^-	f^+	Atom	f^-	f^+
C1	0.001	0.000	C1	0.003	0.006	C1	0.002	0.000
C2	0.000	0.000	C2	0.001	0.016	C2	0.001	0.000
C3	0.001	0.000	C3	0.013	0.007	C3	0.001	0.000
C4	0.000	0.000	C4	0.005	0.000	C4	0.003	0.000
C5	0.001	0.001	C5	0.004	0.003	C5	0.003	0.000
C6	0.002	0.001	C6	0.002	0.002	C6	0.004	0.001
C7	0.003	0.001	C7	0.129	−0.001	C7	0.002	0.001
C8	−0.002	−0.001	C8	0.008	−0.001	C8	−0.002	0.001
C9	0.005	0.001	C9	0.006	0.013	C9	0.004	0.001
C10	0.004	0.001	C10	0.003	0.021	C10	0.002	0.001
C11	0.006	−0.002	C11	0.003	0.000	C11	0.008	−0.003
C12	0.128	0.003	C12	0.001	0.000	C12	0.125	0.003
C13	0.176	0.031	C13	0.029	0.004	C13	0.175	0.024
C14	0.033	0.007	C14	0.159	0.013	C14	0.030	0.005
C15	0.014	0.002	C15	0.001	0.000	C15	0.018	0.008
C16	0.002	0.015	C16	0.001	0.000	C16	0.003	0.014

(*continued on next page*)

Table 6 (*continued*)

Triterpenoid			Euscaphic acid			Ursolic acid		
Atom	f^-	f^+	Atom	f^-	f^+	Atom	f^-	f^+
C17	0.003	0.011	C17	0.004	0.001	C17	0.005	0.005
C18	0.007	0.004	C18	0.004	0.000	C18	0.017	0.001
C19	0.004	0.021	C19	0.001	0.000	C19	0.005	0.023
C20	0.003	0.013	C20	0.001	0.000	C20	0.003	0.005
C21	0.007	0.001	C21	0.003	0.000	C21	0.005	0.001
C22	0.018	0.006	C22	0.003	0.001	C22	0.015	0.000
C23	0.003	0.002	O23	0.013	0.008	C23	0.006	0.004
C24	0.007	0.004	O24	0.007	0.000	C24	0.009	0.003
C25	0.021	0.005	O25	0.003	0.000	C25	0.002	0.203
C26	0.008	0.001	C26	0.004	0.223	O26	0.016	0.225
C27	0.004	0.001	O27	0.018	0.245	O27	0.006	0.108
C28	0.001	0.000	O28	0.012	0.133	C28	0.014	0.009
C29	0.001	0.000	C29	0.006	0.007	C29	0.003	0.002
C30	0.000	0.200	C30	0.008	0.003	C30	0.001	0.000
O31	0.012	0.218	C31	0.022	0.002	C31	0.002	0.000
O32	0.013	0.121	C32	0.008	0.002	C32	0.003	0.001
O33	0.002	0.001	C33	0.004	0.001	O33	0.007	0.000
O34	0.000	0.000	C34	0.002	0.000			
S35	0.001	0.001	C35	0.001	0.000			
O36	0.001	0.001						
O37	0.001	0.001						
O38	0.001	0.000						

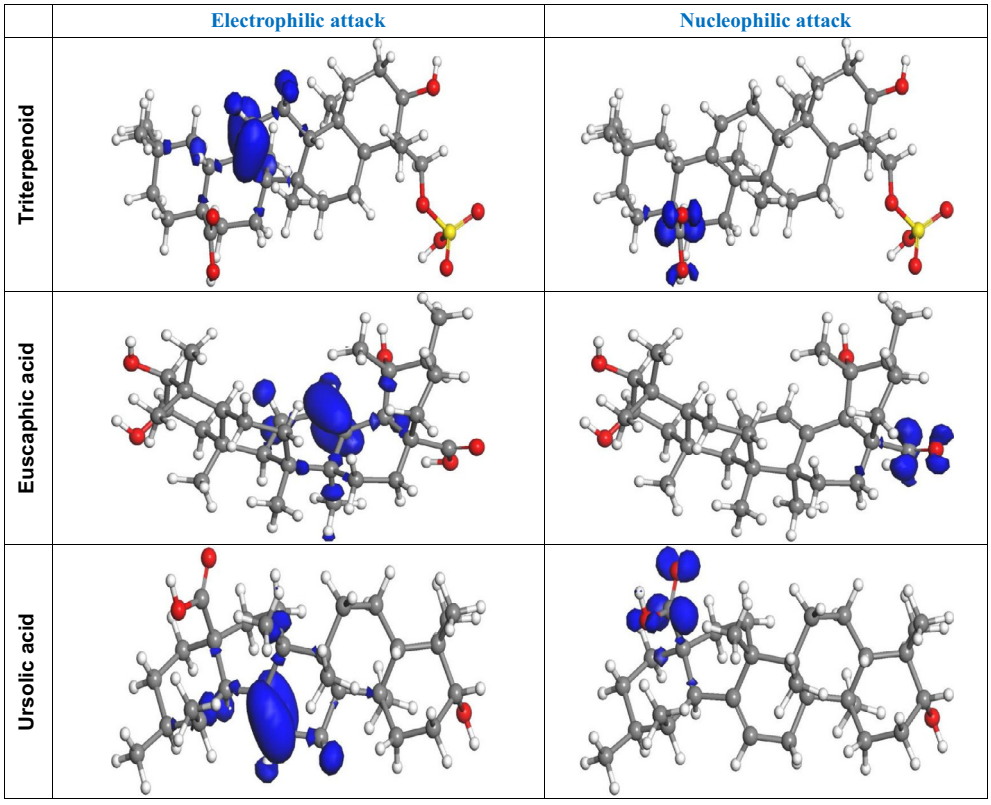

Fig. 12. The simulated Fukui indices of neutral triterpenoid, euscaphic acid, and ursolic acid compounds.

5. Conclusions

Electrochemical and surface characterizations determined the inhibition efficiency of Eriobotrya japonica Lindl (EJL) extract as a biocompatible inhibitor for mild steel in 1 M HCl solution. Due to the electrochemical tests, the organic compounds present in the extract made a protective layer on the surface through chemisorption and physisorption mechanism on the anodic and cathodic sites, respectively. Hence, the EJL extract was classified as a mixed-type inhibitor with the dominant anodic effect which reduced the corrosion rate sufficiently. The most effective concentration was specified at 800 ppm. Production of the inhibitive layer at the metal/electrolyte interface was observed by SEM and AFM micrographs which clarified the least surface destruction in the presence of inhibitor. The measured contact angle between water droplet and mild steel surface also evidenced the formation of the hydrophobic film composed of EJL organic constituents (i.e. ursolic acid and euscaphic acid). The computational outcomes

derived from QM computations and classical simulations clarified the reactivity and adsorption of EJL extract species on steel substrate.

Declaration of Competing Interest

None.

Acknowledgment

The present study was supported by Golestan University, Gorgan, Iran. Authors gratefully thank the use of School of Computer Science, Institute for Research in Fundamental Science (IPM) as the computations were done there.

Appendix A. Supplementary data

Supplementary data to this article can be found online at https://doi.org/10.1016/j.conbuildmat.2019.06.005.

References

[1] A. Ostovari, S. Hoseinieh, M. Peikari, S. Shadizadeh, S. Hashemi, Corrosion inhibition of mild steel in 1 M HCl solution by henna extract: a comparative study of the inhibition by henna and its constituents (Lawsone, Gallic acid, α-d-Glucose and Tannic acid), Corros. Sci. 51 (9) (2009) 1935–1949.
[2] D. Özkır, K. Kayakırılmaz, E. Bayol, A.A. Gürten, F. Kandemirli, The inhibition effect of Azure A on mild steel in 1 M HCl. A complete study: Adsorption, temperature, duration and quantum chemical aspects, Corros. Sci. 56 (2012) 143–152.
[3] N.O. Obi-Egbedi, I.B. Obot, Inhibitive properties, thermodynamic and quantum chemical studies of alloxazine on mild steel corrosion in H2SO4, Corros. Sci. 53 (1) (2011) 263–275.
[4] M. Finšgar, J. Jackson, Application of corrosion inhibitors for steels in acidic media for the oil and gas industry: a review, Corros. Sci. 86 (2014) 17–41.
[5] S. Deng, X. Li, Inhibition by Ginkgo leaves extract of the corrosion of steel in HCl and H2SO4 solutions, Corros. Sci. 55 (2012) 407–415.
[6] M. Mobin, M. Rizvi, Polysaccharide from Plantago as a green corrosion inhibitor for carbon steel in 1 M HCl solution, Carbohydrate Polym. 160 (2017) 172–183.
[7] M.R. Singh, A green approach: a corrosion inhibition of mild steel by Adhatoda vasica plant extract in 0.5 MH 2 SO 4, J. Mater. Environ. Sci. 4 (1) (2013) 119–126.
[8] H. Gerengi, K. Schaefer, H.I. Sahin, Corrosion-inhibiting effect of Mimosa extract on brass-MM55 corrosion in 0.5 M H2SO4 acidic media, J. Ind. Eng. Chem. 18 (6) (2012) 2204–2210.
[9] B. Ramezanzadeh, M. Mehdipour, S.Y. Arman, Application of electrochemical noise to investigate corrosion inhibition properties of some azole compounds on aluminum in 0.25 M HCl, Prog. Color Colorants Coat. 8 (2015) 69–86.
[10] M. Mehdipour, B. Ramezanzadeh, S. Arman, Electrochemical noise investigation of Aloe plant extract as green inhibitor on the corrosion of stainless steel in 1 M H2SO4, J. Ind. Eng. Chem. 21 (2015) 318–327.
[11] M. Jokar, T.S. Farahani, B. Ramezanzadeh, Electrochemical and surface characterizations of morus alba pendula leaves extract (MAPLE) as a green corrosion inhibitor for steel in 1 M HCl, J. Taiwan. Inst. Chem. Eng. 63 (2016) 436–452.
[12] A. Satapathy, G. Gunasekaran, S. Sahoo, K. Amit, P. Rodrigues, Corrosion inhibition by Justicia gendarussa plant extract in hydrochloric acid solution, Corros. Sci. 51 (12) (2009) 2848–2856.
[13] G. Ji, S. Anjum, S. Sundaram, R. Prakash, Musa paradisica peel extract as green corrosion inhibitor for mild steel in HCl solution, Corros. Sci. 90 (2015) 107–117.
[14] Z. Zhang, H. Ba, Z. Wu, Y. Zhu, The inhibition mechanism of maize gluten meal extract as green inhibitor for steel in concrete via experimental and theoretical elucidation, Constr. Build. Mater. 198 (2019) 288–298.
[15] C.-H. Lee, S.-L. Wu, J.-C. Chen, C.-C. Li, H.-Y. Lo, W.-Y. Cheng, et al., Eriobotrya japonica leaf and its triterpenes inhibited lipopolysaccharide-induced cytokines and inducible enzyme production via the nuclear factor-κB signaling pathway in lung epithelial cells, Am. J. Chin. Med. 36 (06) (2008) 1185–1198.
[16] H.A. Jung, J.C. Park, H.Y. Chung, J. Kim, J.S. Choi, Antioxidant flavonoids and chlorogenic acid from the leaves ofEriobotrya japonica, Arch. Pharmacal Res. 22 (2) (1999) 213.
[17] E.N. Li, J.G. Luo, L.Y. Kong, Qualitative and quantitative determination of seven triterpene acids in Eriobotrya japonica Lindl. by high-performance liquid chromatography with photodiode array detection and mass spectrometry, Phytochem Anal. 20 (4) (2009) 338–343.
[18] J. Shi, W. Chen, X. Zou, Y. Xu, X. Huang, Y. Zhu, et al., Detection of triterpene acids distribution in loquat (Eriobotrya japonica) leaf using hyperspectral imaging, Spectrochim. Acta Part A Mol. Biomol. Spectrosc. 188 (2018) 436–442.
[19] X.-H. Xu, Q. Su, Z.-H. Zang, Simultaneous determination of oleanolic acid and ursolic acid by RP-HPLC in the leaves of Eriobotrya japonica Lindl, J. Pharm. Anal. 2 (3) (2012) 238–240.
[20] Wu. Y-x, Jian T-y, H. Lv, Ding X-q, Zuo Y-y, Ren B-r, et al., Antitussive and expectorant properties of growing and fallen leaves of loquat (Eriobotrya japonica), Rev. Bras. Farmacognosia. 28 (2) (2018) 239–242.
[21] L.O. Olasunkanmi, I.B. Obot, M.M. Kabanda, E.E. Ebenso, Some quinoxalin-6-yl derivatives as corrosion inhibitors for mild steel in hydrochloric acid: experimental and theoretical studies, J. Phys. Chem. C 119 (28) (2015) 16004–16019.
[22] E.D. Raczyńska, K. Woźniak, E. Dolecka, M. Darowska, Superbasic properties of the S N functional group, J. Phys. Org. Chem. 15 (10) (2002) 706–711.
[23] M. Makowski, E.D. Raczyńska, L. Chmurzyński, Ab Initio study of possible and preferred basic site (s) in Polyfunctional N, N 1-Dimethyl-N-cyanoformamidine, J. Chem. Phys. A 105 (5) (2001) 869–874.
[24] E.D. Raczynska, M. Darowska, I. Dabkowska, M. Decouzon, J.-F. Gal, P.-C. Maria, et al., Experimental and theoretical evidence of basic site preference in polyfunctional superbasic amidinazine: N 1, N 1-Dimethyl-N 2-β-(2-pyridylethyl) formamidine, J. Org Chem. 69 (12) (2004) 4023–4030.
[25] E.D. Raczynska, M. Makowski, E. Gornicka, M. Darowska, Ab Initio studies on the preferred site of protonation in cytisine in the gas phase and water, Int. J. Mol. Sci. 6 (1) (2005) 143–156.
[26] P.C. Hariharan, J.A. Pople, The influence of polarization functions on molecular orbital hydrogenation energies, Theor. Chim. Acta 28 (3) (1973) 213–222.
[27] A.D. Becke, Density-functional thermochemistry. III. The role of exact exchange, J. Chem. Phys. 98 (7) (1993) 5648–5652.
[28] C. Lee, W. Yang, R.G. Parr, Development of the Colle-Salvetti correlation-energy formula into a functional of the electron density, Phys. Rev. B. 37 (2) (1988) 785–789.
[29] A.D. McLean, G.S. Chandler, Contracted Gaussian basis sets for molecular calculations. I. Second row atoms, Z=11–18, J. Chem. Phys. 72 (10) (1980) 5639–5648.
[30] P. Hohenberg, W. Kohn, Inhomogeneous Electron Gas, Phys. Rev. 136 (3B) (1964) B864–B871.
[31] W. Kohn, L.J. Sham, Self-consistent equations including exchange and correlation effects, Phys. Rev. 140 (4A) (1965) A1133–A1138.
[32] J. Tomasi, B. Mennucci, R. Cammi, Quantum mechanical continuum solvation models, Chem. Rev. 105 (8) (2005) 2999–3094.
[33] , Gaussian 09, revision D. 01. Gaussian, Inc., Wallingford CT, 2009.
[34] C.M. Breneman, K.B. Wiberg, Determining atom-centered monopoles from molecular electrostatic potentials. The need for high sampling density in formamide conformational analysis, J. Comput. Chem. 11 (3) (1990) 361–373.
[35] K. Khaled, Studies of iron corrosion inhibition using chemical, electrochemical and computer simulation techniques, Electrochim. Acta. 55 (22) (2010) 6523–6532.
[36] N. Kovačević, A. Kokalj, Analysis of molecular electronic structure of imidazole- and benzimidazole-based inhibitors: a simple recipe for qualitative estimation of chemical hardness, Corros. Sci. 53 (3) (2011) 909–921.
[37] S.K. Saha, P. Ghosh, A. Hens, N.C. Murmu, P. Banerjee, Density functional theory and molecular dynamics simulation study on corrosion inhibition performance of mild steel by mercapto-quinoline Schiff base corrosion inhibitor, Physica E 66 (2015) 332–341.
[38] A.Y. Musa, R.T. Jalgham, A.B. Mohamad, Molecular dynamic and quantum chemical calculations for phthalazine derivatives as corrosion inhibitors of mild steel in 1M HCl, Corros. Sci. 56 (2012) 176–183.
[39] S. John, M. Kuruvilla, A. Joseph, Adsorption and inhibition effect of methyl carbamate on copper metal in 1 N HNO3: an experimental and theoretical study, RSC Adv. 3 (23) (2013) 8929–8938.
[40] S.K. Saha, M. Murmu, N.C. Murmu, P. Banerjee, Evaluating electronic structure of quinazolinone and pyrimidinone molecules for its corrosion inhibition effectiveness on target specific mild steel in the acidic medium: a combined DFT and MD simulation study, J. Mol. Liq. 224 (2016) 629–638.
[41] J.P. Perdew, K. Burke, M. Ernzerhof, Generalized gradient approximation made simple, Phys. Rev. Lett. 77 (18) (1996) 3865.
[42] J. Fu, H. Zang, Y. Wang, S. Li, T. Chen, X. Liu, Experimental and theoretical study on the inhibition performances of quinoxaline and its derivatives for the corrosion of mild steel in hydrochloric acid, Ind. Eng. Chem. Res. 51 (18) (2012) 6377–6386.
[43] A. Dutta, S.K. Saha, P. Banerjee, D. Sukul, Correlating electronic structure with corrosion inhibition potentiality of some bis-benzimidazole derivatives for mild steel in hydrochloric acid: Combined experimental and theoretical studies, Corros. Sci. 98 (2015) 541–550.
[44] C. Verma, L.O. Olasunkanmi, E.E. Ebenso, M.A. Quraishi, I.B. Obot, Adsorption behavior of glucosamine-based, pyrimidine-fused heterocycles as green corrosion inhibitors for mild steel: experimental and theoretical studies, J. Phys. Chem. C. 120 (21) (2016) 11598–11611.
[45] P. Singh, E.E. Ebenso, L.O. Olasunkanmi, I.B. Obot, M.A. Quraishi, Electrochemical, theoretical, and surface morphological studies of corrosion inhibition effect of green naphthyridine derivatives on mild steel in hydrochloric acid, J. Phys. Chem. C. 120 (6) (2016) 3408–3419.
[46] M.J. Palimi, E. Alibakhshi, B. Ramezanzadeh, G. Bahlakeh, M. Mahdavian, Screening the anti-corrosion effect of a hybrid pigment based on zinc acetyl

acetonate on the corrosion protection performance of an epoxy-ester polymeric coating, J. Taiwan Inst. Chem. Eng. 82 (2018) 261–272.
[47] B. Xu, W. Gong, K. Zhang, W. Yang, Y. Liu, X. Yin, et al., Theoretical prediction and experimental study of 1-Butyl-2-(4-methylphenyl)benzimidazole as a novel corrosion inhibitor for mild steel in hydrochloric acid, J. Taiwan Inst. Chem. Eng. 51 (2015) 193–200.
[48] S. Kaya, L. Guo, C. Kaya, B. Tüzün, I.B. Obot, R. Touir, et al., Quantum chemical and molecular dynamic simulation studies for the prediction of inhibition efficiencies of some piperidine derivatives on the corrosion of iron, J. Taiwan Inst. Chem. Eng. 65 (2016) 522–529.
[49] Accelrys Software Inc. SD, 2009.
[50] H. Sun, COMPASS: An ab initio force-field optimized for condensed-phase applications overview with details on alkane and benzene compounds, J. Phys. Chem. B 102 (38) (1998) 7338–7364.
[51] H. Sun, P. Ren, J. Fried, The COMPASS force field: parameterization and validation for phosphazenes, Comput. Theor. Polym. Sci. 8 (1) (1998) 229–246.
[52] E. Alibakhshi, M. Ramezanzadeh, G. Bahlakeh, B. Ramezanzadeh, M. Mahdavian, M. Motamedi, Glycyrrhiza glabra leaves extract as a green corrosion inhibitor for mild steel in 1 M hydrochloric acid solution: Experimental, molecular dynamics, Monte Carlo and quantum mechanics study, J. Mol Liq. 255 (2018) 185–198.
[53] W.C. Swope, H.C. Andersen, P.H. Berens, K.R. Wilson, A computer simulation method for the calculation of equilibrium constants for the formation of physical clusters of molecules: application to small water clusters, J. Chem. Phys. 76 (1) (1982) 637–649.
[54] G.J. Martyna, M.L. Klein, M. Tuckerman, Nosé-Hoover chains: the canonical ensemble via continuous dynamics, J. Chem. Phys. 97 (4) (1992) 2635–2643.
[55] S. Nose, An extension of the canonical ensemble molecular dynamics method, Mol. Phys. 57 (1) (1986) 187–191.
[56] Z. Sanaei, T. Shahrabi, B. Ramezanzadeh, Synthesis and characterization of an effective green corrosion inhibitive hybrid pigment based on zinc acetate-Cichorium intybus L leaves extract (ZnA-CIL. L): electrochemical investigations on the synergistic corrosion inhibition of mild steel in aqueous chloride solutions, Dyes Pigm. 139 (2017) 218–232.
[57] A. Gómez-Siurana, A. Marcilla, M. Beltrán, D. Berenguer, I. Martínez-Castellanos, S. Menargues, TGA/FTIR study of tobacco and glycerol–tobacco mixtures, Thermochim. Acta 573 (2013) 146–157.
[58] S. Xue, Q. Zhao, X. Ma, F. Li, J. Wang, L. Wei, Comparison of dissolved organic matter fractions in a secondary effluent and a natural water, Environ. Monit. Assess. 180 (1–4) (2011) 371–383.
[59] E. Salehi, R. Naderi, B. Ramezanzadeh, Synthesis and characterization of an effective organic/inorganic hybrid green corrosion inhibitive complex based on zinc acetate/Urtica Dioica, Appl. Surf. Sci. 396 (2017) 1499–1514.
[60] P. Mourya, S. Banerjee, M. Singh, Corrosion inhibition of mild steel in acidic solution by Tagetes erecta (Marigold flower) extract as a green inhibitor, Corros Sci. 85 (2014) 352–363.
[61] N. Soltani, N. Tavakkoli, M. Khayatkashani, M.R. Jalali, A. Mosavizade, Green approach to corrosion inhibition of 304 stainless steel in hydrochloric acid solution by the extract of Salvia officinalis leaves, Corros. Sci. 62 (2012) 122–135.
[62] G. Bahlakeh, M. Ramezanzadeh, B. Ramezanzadeh, Experimental and theoretical studies of the synergistic inhibition effects between the plant leaves extract (PLE) and zinc salt (ZS) in corrosion control of carbon steel in chloride solution, J. Mol. Liq. 248 (2017) 854–870.
[63] J. Zhang, G. Qiao, S. Hu, Y. Yan, Z. Ren, L. Yu, Theoretical evaluation of corrosion inhibition performance of imidazoline compounds with different hydrophilic groups, Corros. Sci. 53 (1) (2011) 147–152.
[64] K. Anupama, K. Ramya, A. Joseph, Electrochemical and computational aspects of surface interaction and corrosion inhibition of mild steel in hydrochloric acid by Phyllanthus amarus leaf extract (PAE), J. Mol. Liq. 216 (2016) 146–155.
[65] S. John, J. Joy, M. Prajila, A. Joseph, Electrochemical, quantum chemical, and molecular dynamics studies on the interaction of 4-amino-4H, 3, 5-di (methoxy)-1, 2, 4-triazole (ATD), BATD, and DBATD on copper metal in 1N H2SO4, Mater. Corros. 62 (11) (2011) 1031–1041.